

Article

Incipient Motion of Bed Material in a Channel with Varying Width and Vegetated Channel Walls

Sanaz Hadian ¹, Hossein Afzalimehr ^{1,*} and Jueyi Sui ^{2,*}

¹ School of Civil Engineering, Iran University of Science and Technology, Tehran 16846-13114, Iran; sanaz_hadian@civileng.iust.ac.ir

² School of Engineering, University of Northern British Columbia, Prince George, BC V2N 4Z9, Canada

* Correspondence: hafzali@iust.ac.ir (H.A.); jueyi.sui@unbc.ca (J.S.)

Abstract: This experimental study aims to investigate the characteristics of turbulent flow in channels with vegetated banks and varying channel width under the condition of the incipient motion of bed material. The natural reeds were used as emergent vegetation on the sidewalls of a laboratory flume. In total, nine experimental runs have been conducted with different experimental setups by using three different particle sizes of bed material and three different channel bed slopes. An Acoustic Doppler velocimetry (ADV) was used to acquire velocity components in three directions. The results of this study indicate that the streamwise velocities have the maximum and minimum values at the cross sections with the narrowest and widest width, respectively. When the aspect ratio is less than 5, the maximum velocity occurs below the water surface, due to presence of the secondary currents. It is found that, at all measurement points, the distribution of the Reynolds shear stress has a Z-shaped profile owing to presence of vegetation on the channel sidewalls. By extrapolating the profiles for flow velocity and Reynolds shear stress towards the surface of the channel bed, the near-bed incipient velocities and the corresponding shear stresses for the incipient motion have been determined. By increasing the channel bed slope, the estimated near-bed parameters for all particle sizes decreased, indicating the dominance of the gravity effect over the pressure gradient effect. It was also observed that the Shields method was invalid for assessing the incipient motion of bed material in the presence of vegetation on the sidewalls of a channel that has a varying width.

Keywords: varying channel width; emergent vegetation; incipient motion; near-bed velocity; shear stress; Shields method



Citation: Hadian, S.; Afzalimehr, H.; Sui, J. Incipient Motion of Bed Material in a Channel with Varying Width and Vegetated Channel Walls. *Water* **2023**, *15*, 3691. <https://doi.org/10.3390/w15203691>

Academic Editor: Bommanna Krishnappan

Received: 4 October 2023

Revised: 18 October 2023

Accepted: 20 October 2023

Published: 22 October 2023



Copyright: © 2023 by the authors. Licensee MDPI, Basel, Switzerland. This article is an open access article distributed under the terms and conditions of the Creative Commons Attribution (CC BY) license (<https://creativecommons.org/licenses/by/4.0/>).

1. Introduction

The incipient motion of sediment in a channel bed plays a key role in many river engineering projects, such as design of stable channels, estimation of riverbed resistance, prevention of scouring and sedimentation processes [1]. Generally, the width of natural channels varies, thus leading to non-uniform flow in rivers and stream. The presence of vegetation patches in natural rivers either on channel beds or channel banks or both is inevitable, especially in small rivers and streams. On the one hand, the presence of vegetation in a channel increases the flow resistance and thus reduces the possibility of sediment transport, and on the other hand, it decreases the threshold velocity for lifting the particles owing to the increase of turbulence intensities [2,3]. Considering the above-mentioned complicated process, it is essential to assess the effects of vegetation on the incipient motion of bed material.

Laboratory experiments can aid researchers to evaluate different aspects of fluvial hydraulics under controlled hydraulic and boundary conditions. In this regard, many experimental works have been performed in order to assess the condition for the incipient motion of bed material by changing hydraulic parameters. Generally, the threshold condition can be investigated by two approaches: the bed-load extrapolation approach and the

visual observation approach [4]. In the extrapolation approach, the critical shear stress is determined by extrapolating the bed shear stress either to the null or to the low reference value of sediment transport flux [5]. This approach is sensitive to the extrapolation and the reference value [6]. The visual observation approach, however, is based upon the monitoring of particle movements.

Kramer [7] classified four categories for sediment motions: (1) no sediment transport—without movement of sediment particles; (2) weak sediment transport—with movement of a small number of the smallest particles in the specified part of a channel bed; (3) medium sediment transport—with movement of a large number of medium-sized particles; and (4) general sediment transport—with the motion of particles of all sizes in all parts of a channel bed. Some researchers pointed out that sediment movements were affected by the near-bed turbulence, which describes the nature of the hydrodynamic forces acting on sediment particles [8]. On the other hand, it was reported that the threshold velocity for the incipient motion of bed material was directly influenced by both particle size and flow depth [9]. The threshold values of the near-bed velocity and shear stress are the velocity and shear stress values at the channel bed surface under the defined threshold condition [4]. By considering flow depth and sediment characteristics, some equations have been developed for calculating these threshold values [10–13].

The criterion proposed by Shield [14] is the most important and widely used approach for assessing the incipient motion of bed material. In the Shields diagram the movements of sediment particles can be assessed by using the critical shear Reynolds number and Shields dimensionless parameter. When a data point lies on the Shields curve, it indicates the “incipient motion” condition. Points located below and above the curve represent “no sediment motion” and “sediment motion” condition, respectively. However, it was proved later that the critical Shields stress for the incipient motion of particles deviates from the Shields curve, due to some uncertainties in calculating the bed shear stress, in case of the presence of non-uniform flow, as well as the differences in definition of the threshold condition [5,15,16].

The presence of vegetation in rivers affects various aspects of the environment and aquatic systems, such as banks stability, sediment transport, water quality, and aquatic habitats. To address issues regarding river restoration and water conservation projects, the impacts of vegetation in rivers have attracted a lot of attention from researchers [17,18]. Tang et al. [19] claimed that due to generation of secondary currents resulted from vegetation in the channel bed, the velocity for the incipient motion of bed material declined. Also, the impacts of the density of emergent vegetation on sediment transport were investigated. It was found that the threshold velocity decreased by increasing the stem density along the channels [20]. Shahmohammadi et al. claimed that the submerged vegetation patches affect the motion of bed material [9]. The results showed that the presence of vegetation along the flow greatly influences the condition for the incipient motion of bed material, Reynolds shear stress and kinetic energy distributions. Moreover, the average incipient velocity decreased by 20%, compared to that in a bare channel. In a channel with vegetated sidewalls and gravel bed, it is found that the presence of vegetation led to the change in the location of the maximum shear stress. Furthermore, by reducing the median size of bed material, less change in Reynolds shear stress was recognized [21]. To better understand the mechanisms of fluids transport through fibrous porous media, by using analytical solutions and numerical simulations, several studies were performed [22,23]. However, in experimental studies with fine particles as bed material, it is assumed that the bed permeability is negligible.

Several studies were carried out to determine the effects of variation in channel width on the morphodynamics and flow structures [24–26]. It was found that the contraction of a channel controls the acceleration and deceleration of the flow, leading to the generation of turbulence. Turbulence eddies formed in the flow separation zones influence the velocity and shear stress patterns [27]. It was reported that the channel width and change of the bedform wavelength were known as key factors influencing the sequence of bedforms [28].

In a field study in the Babolroud River, it was found that the velocity vector oriented in different directions at various locations of bedforms that were caused by the variation of channel width and flow non-uniformity [29]. To date, the same numerical models have also been developed to examine the effects of the variation of channel width on the bedload transport, bedform maintenance and cyclic erosion/deposition [30–33]. In the two-dimensional morphodynamic simulation performed by Morgan [25], the channel width variation amplitude was discovered to be the key control factor for the topographic relief between bedforms. Another numerical study was conducted to investigate the discrete cyclic erosion/deposition regions in channels with varying channel width [34].

By reviewing the above-mentioned studies, it can be concluded that the channel geometry greatly affects sediment transport. Also, the presence of vegetation influences the turbulence patterns, and thus particle movements in a vegetated channel. The incipient motion of bed particles is a stochastic phenomenon and subsequently leads to sediment transport and erosion processes; therefore, a detailed investigation under a controlled experimental environment could lead to concise findings. Resultantly, it is necessary to conduct a deeper investigation of the simultaneous effects of vegetated walls and varying channel width on the characteristics of turbulent flow under the condition of the incipient motion of bed material, which has not been explored up to date and is the main objective of the present innovative study.

2. Materials and Methods

In the current research, experiments were conducted in a laboratory flume that is 11.25 m long, 0.9 m wide, and 0.7 m deep. In the upstream section of the flume, there is a stilling basin with a bar screen which helps the flow dissipate energy after entering into the flume and maintains it to reach a fully developed flow along the flume section for experimentation. The tailgate located at the downstream end of the flume was used to regulate the water depth in the flume. An ADV (Acoustic Doppler Velocimeter), which has an accuracy of 0.001, was used to measure the instantaneous velocity components in three directions (x-streamwise, y-transverse, and z-vertical directions) at different cross sections along the flume and at different distances from the channel sidewall. The channel with varying widths was prepared using Polyvinyl Chloride (PVC) barriers of different diameters (from the minimum diameter of 0.22 m to the maximum diameter of 1.2 m) and covered with a transparent fibrous sheet. The reeds were used to model natural vegetation. Each reed element has an average diameter of 10 mm. The rows of reeds were used as emergent natural vegetation and placed uniformly on both sidewalls of the flume. To compare results of previous studies and incipient conditions [15,16], three sands with different median particle size of 0.56 mm (d_I), 0.74 mm (d_{II}), and 1.08 mm (d_{III}) were used in this study. The particle uniformity is generally estimated by the geometric standard deviation coefficient, defined as $\sigma_g = \left(\frac{d_{84}}{d_{16}}\right)^{\frac{1}{2}}$, where d_{84} and d_{16} are the diameters of the bed particles of which 84% and 16% are finer than them, respectively. As the calculated σ_g was less than 1.4, the sediment particles used in this study belong to the uniform sand [4]. It should be noted that the visual observation approach was employed for distinguishing the bed particle movements. In this regard, the “medium sediment transport” classified by Kramer was considered for particle movements. In this experimental study, the discharge was kept as constant. By adjusting the tailgate at the downstream end of the flume, the water level was lowered until the mentioned criteria for the incipient motion of bed material was achieved. Then, the measurements were conducted. Figure 1 shows the construction steps of the channel with varying width and vegetated sidewalls. Figure 2 presents the grain size distributions for three different bed materials.

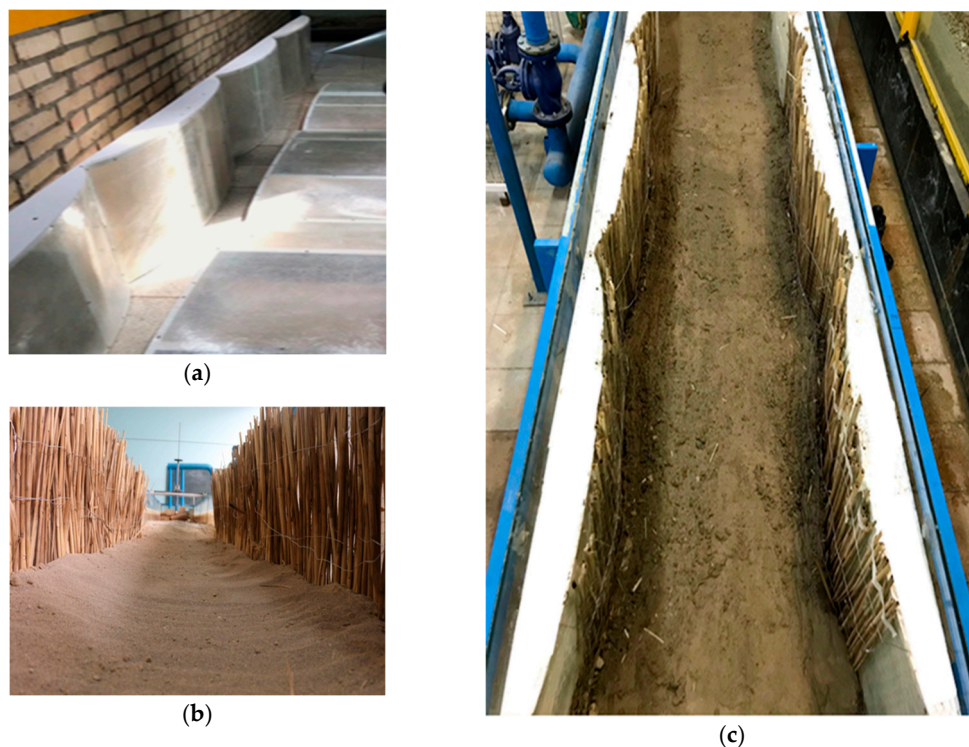


Figure 1. The construction steps of varying width of the experimental flume; (a) the PVC barriers, (b) The row of reeds, as the wall vegetation, (c) the experimental flume with variable width and vegetated walls.

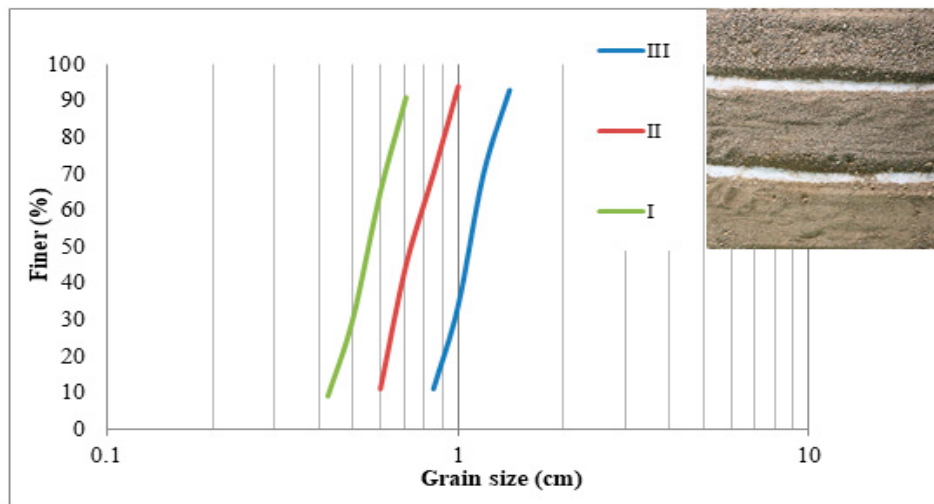


Figure 2. Grain size distributions for three bed materials.

As shown in Figure 3, to investigate the effects resulting from the variation of channel width and vegetation on the sidewalls, measurements were conducted at 9 places along three longitudinal axes (central axis or “C”-axis, “CC”-axis, which is 15 cm from the “C”-axis, and “CCC”-axis, which is 30 cm from the “C”-axis) and at three cross sections (Figure 3–red points). It should be noted that the ADV measurements were conducted in the flume section that is 8 m downstream from the flume entrance, where the flow is fully developed turbulent flow. Table 1 summarizes the conditions for different experimental setups. One can see from Table 1 that the experiments were carried out using three different sands as the bed material with three different slopes of the channel bed.

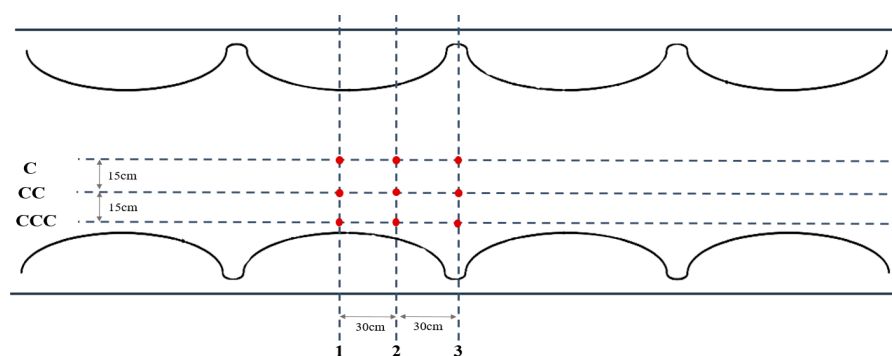


Figure 3. The locations for data acquisitions.

Table 1. The summary of experimental setups.

Experimental Setup	Hydraulic Parameters			
	Discharge (lit/s)	Water Depth (cm)	Froude Number (Fr)	Reynolds Number $Re \times 10^5$
$d_{50} = 0.56 \text{ mm}, S = 0$	27	20	0.12	0.35
$d_{50} = 0.74 \text{ mm}, S = 0$	27	14	0.21	0.34
$d_{50} = 1.08 \text{ mm}, S = 0$	27	12	0.26	0.34
$d_{50} = 0.56 \text{ mm}, S = 0.0075$	27	22	0.11	0.34
$d_{50} = 0.74 \text{ mm}, S = 0.0075$	27	16	0.17	0.35
$d_{50} = 1.08 \text{ mm}, S = 0.0075$	27	13	0.23	0.34
$d_{50} = 0.56 \text{ mm}, S = 0.015$	27	23	0.1	0.35
$d_{50} = 0.74 \text{ mm}, S = 0.015$	27	21	0.11	0.35
$d_{50} = 1.08 \text{ mm}, S = 0.015$	27	14	0.21	0.34

In total, 9 laboratory experiments have been carried out in the current study. The setups for these experiments differ from natural channels. Thus, the following limitations for this conceptual experimental study should be mentioned:

- The flows are steady and non-uniform;
- The change of the channel width in the streamwise direction is symmetric;
- The diameters of all reed elements are the same;
- The density of inflexible vegetation on the sidewalls is kept as constant.

3. Results and Discussion

In this section, to avoid repetition, the results for experimental setups with the minimum and maximum slopes of the channel bed with both the finest and the coarsest particles are reported:

3.1. Results in the Flat Channel

3.1.1. Streamwise Velocity Distribution

The distribution of streamwise velocity component (u) for the finest sand ($d_{50} = 0.56 \text{ mm}$) is shown in Figure 4. One can see from Figures 4 and 5 that the streamwise velocity had the largest and lowest values, respectively, at cross Section 1 (CS-1) (with the minimum channel width) and CS-3 (with the maximum channel width) along all three longitudinal axes (C-axis, CC-axis and CCC-axis). The velocity values along the C-axis were also higher than those along other two axes, according to the non-slipping principle. Furthermore, since the aspect ratio (w/h) is less than 5, the location of the maximum velocity occurred below the water surface. This phenomenon, which is defined as “dip”, occurs in three dimensional flows and narrow channels due to the presence of secondary currents [35]. It was reported

in previous works [21,36] that the vegetated sidewalls of a channel play a major role in generating secondary currents. In this study, the vegetated sidewalls and the varying width of the channel lead to the development of secondary currents; hence, the “dip” phenomenon appears in most velocity profiles. As showed in Figure 5, for the smaller aspect ratios, the velocity profiles along all axes were clearly affected. In contrast, for larger aspect ratios, the effects of channel banks and secondary currents limit the zone near the channel walls; and thus, the dip phenomenon would not be observed along the central C-axis. At CS-1, where the channel width and the aspect ratio are the least, the “dip” phenomenon occurred along the central C-axis (Figure 4a); but with the increase in the channel width, the “dip” phenomenon was not observed along the central C-axis (Figure 4b,c).

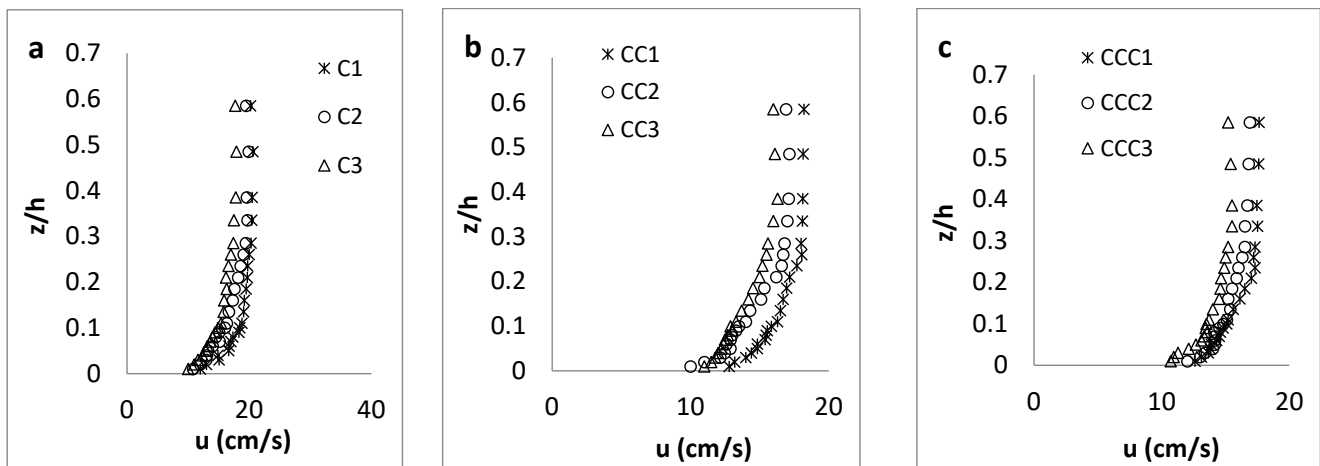


Figure 4. (a–c) Streamwise velocity distributions (experimental setup: $S = 0$, $d_{50} = 0.56$ mm).

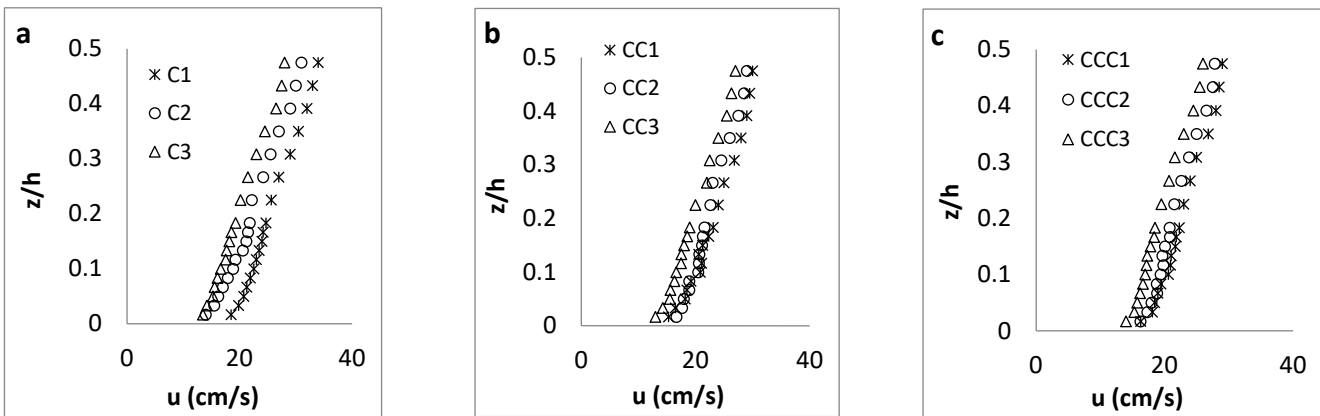


Figure 5. (a–c) Streamwise velocity distributions (experimental setup: $S = 0$, $d_{50} = 1.08$ mm).

As presented in Figure 5 for the channel with the coarsest sand as the bed material, the streamwise velocity along all three longitudinal axes (C-axis, CC-axis and CCC-axis) had the maximum and minimum values, respectively, at CS-1 and CS-3, similar to the results for experimental setup with the finest sand. Velocity values along the central C-axis were also higher than those along other two axes closer to the channel sidewall, according to the non-slipping principle. In addition, the “dip” phenomenon was not observed in any of velocity profiles, since the aspect ratio is larger than 5 [35].

3.1.2. Turbulence Intensity Distribution

According to Grass [37], the maximum value of u_{rms} ($u_{rms} = \sqrt{u'^2}$) occurs at a the flow depth of $0.04 h \sim 0.12 h$ from the bed surface, (where h is the water depth), and has less values

in higher depths near the water surface. The result of u_{rms} distribution in this study had a convex shape, regardless of the particle sizes of the bed material (Figures 6 and 7). It was also observed that the turbulence intensities along the central C-axes had the lowest values, and showed an increasing trend by moving towards the channel sidewalls. In other words, the channel sidewalls and wall vegetation had a major role in producing turbulence eddies, and increased turbulence intensities. This finding was also reported in previous works conducted in channels with the varying channel width [29,38], as well as either submerged or emergent vegetation in channels [9,21,39].

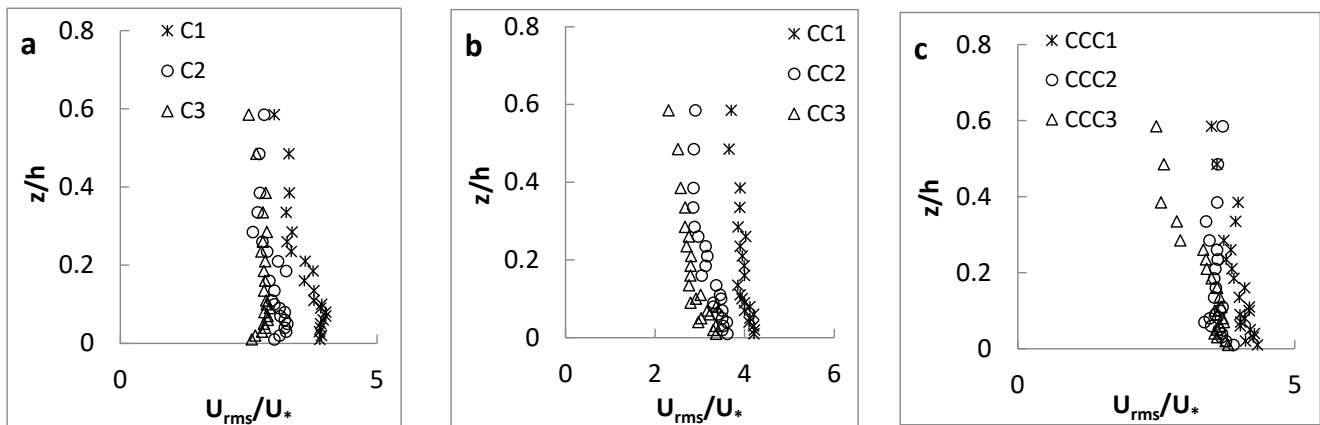


Figure 6. (a–c) Turbulence intensity distributions (experimental setup: $S = 0$, $d_{50} = 0.56$ mm).

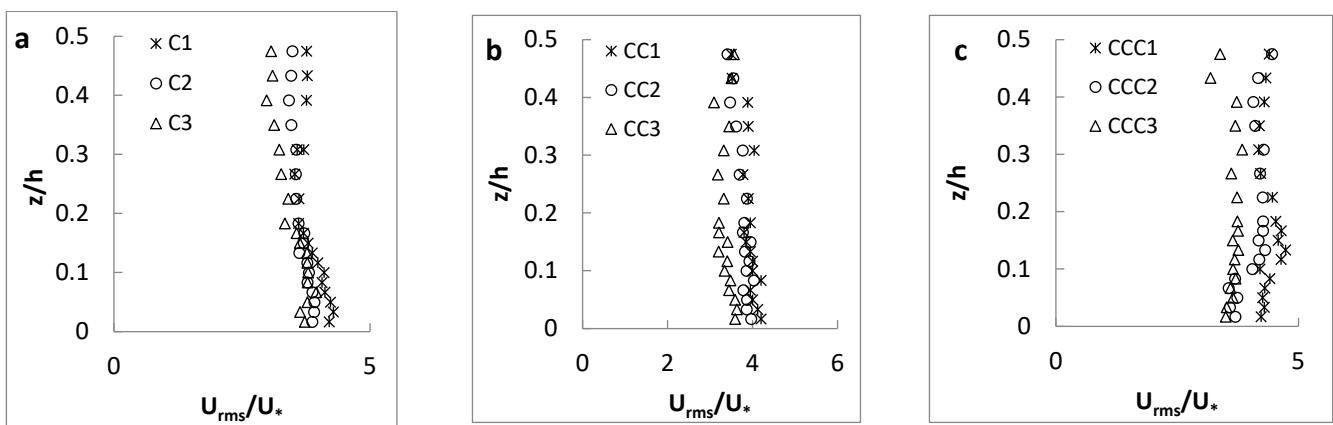


Figure 7. (a–c) Turbulence intensity distributions (experimental setup: $S = 0$, $d_{50} = 1.08$ mm).

3.1.3. Reynolds Shear Stress

The results showed that since both $(u'v')$ and $(v'w')$ had small values without any significant changes, regardless of experimental setups for all experiments, the results of $(u'w')$ which is the most predominant component of the shear stress are discussed here. For bed particles with weak movements, according to Nikora and Goring [40], the dimensionless Reynolds shear stress profile is divided into three regions throughout the flow depth. In the first region near the bed surface, the shear stress profile starts from a non-zero value, and then increases until reaches its maximum value at the flow depth of $z/h \cong 0.3$, which is the boundary between regions 1 and 2. The profile then has a decreasing trend in region 2, and reaches its minimum value (close to zero) at the boundary between regions 2 and 3. In the current study, due to the limitation of ADV measurements that can only be conducted 5 cm below the water surface, investigating Reynolds shear stress in region 3, which is a thin layer, is not possible.

For flow in the channel with the finest sand, all profiles of Reynolds shear stress had a convex shape (Figure 8). However, the maximum values of Reynolds shear stress at

CS-1 occurred at a smaller distance near the bed. Additionally, the maximum values of Reynolds shear stress had the largest and smallest value at CS-1 and CS-3, respectively.

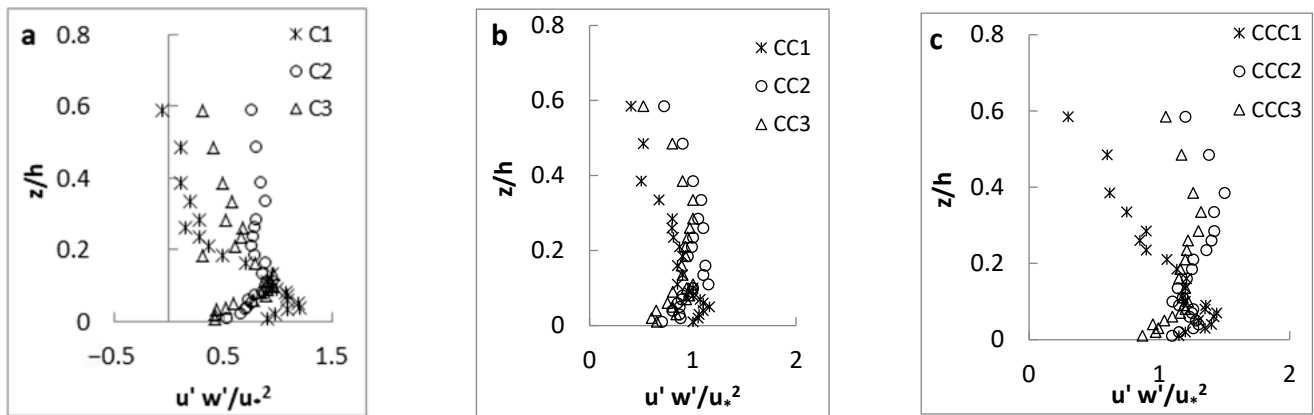


Figure 8. (a–c) Reynolds shear stress distributions (experimental setup: $S = 0$, $d_{50} = 0.56$ mm).

The interaction of the wall vegetation and the varying width of the channel affects the distribution patterns of Reynolds shear stress. Results showed that the shear stress profiles had four distinct zones and had a Z-shape distribution at CS-2 and CS-3, where the flow along this section from CS-2 to CS-3 belongs to a decelerating flow. Resultantly, the presence of vegetation on the channel sidewalls caused the formation of different shear layers with complex behaviors, especially near the vegetation on the sidewalls. For this case, the maximum values of Reynolds shear stress occurred at the flow depth of $0.3 < z/h < 0.4$ from the bed surface. A similar pattern of Reynolds shear stress distribution was also reported in other studies [21,36] in which the impacts of the wall vegetation on flow structures were examined. Moreover, the shear stress had the largest values in the vicinity of vegetation and the maximum values occurred at the flow depth of $z/h \cong 0.4$ from the bed surface (Figure 8c).

The distribution of Reynolds shear stress for flow in the channel with the coarsest sand also had a Z-shape pattern, similar to the results for the experimental setup with the finest sand (Figure 9). One can conclude from Figures 9 and 10 that by increasing the grain size of bed material, the shear stress values increased, and the maximum value of shear stress occurred closer to the bed surface. This result agrees with that of Shahmohammadi et al. [9] who did experiments with a sand bed with a medium motion of particles by changing the grain sizes of bed material.

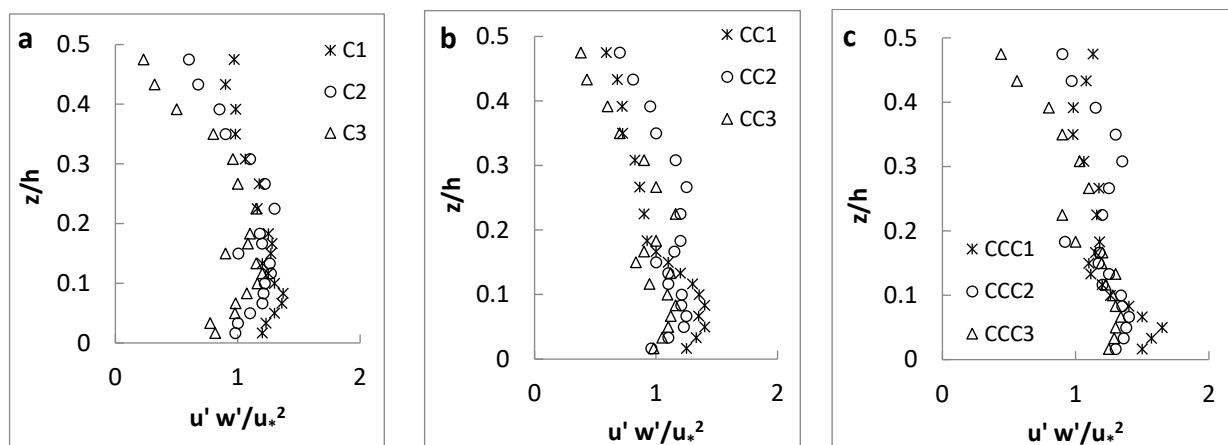


Figure 9. (a–c) Reynolds shear stress distributions (experimental setup: $S = 0$, $d_{50} = 1.08$ mm).

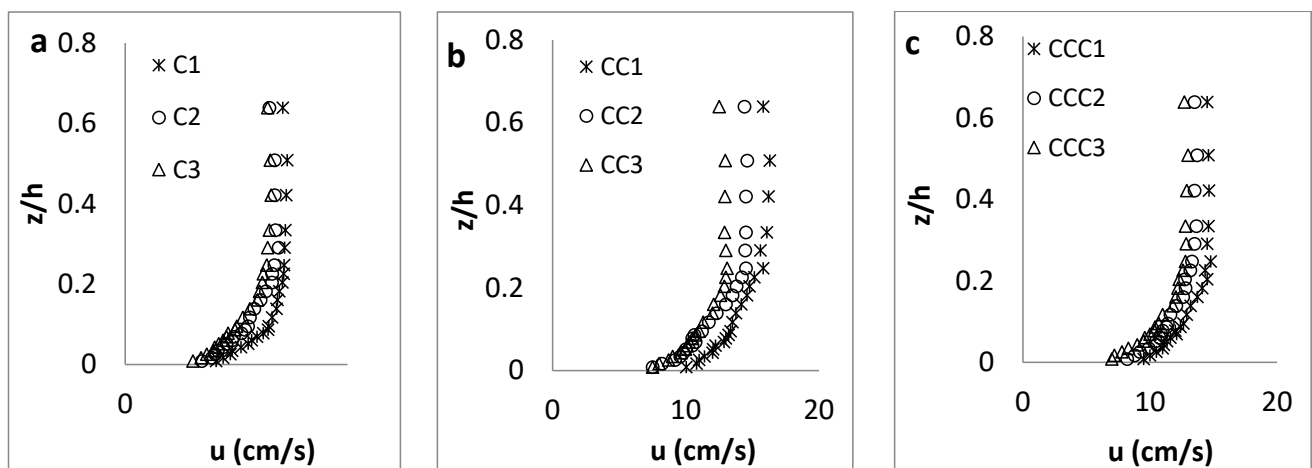


Figure 10. (a–c) Streamwise velocity distributions (experimental setup: $S = 0.015$, $d_{50} = 0.56$ mm).

3.2. Results in the Steepest Channel

3.2.1. Streamwise Velocity Distribution

As indicated in Figures 10 and 11, the trends of streamwise velocity profiles are similar to those of the experimental setup with a flat channel bed ($S = 0$). The “dip” phenomenon was observed in most velocity profiles in the channel with the finest sand, and was more tangible at CS-1, where the channel width is the least and thus the lowest aspect ratio (Figure 10). For the channel with the coarsest sand, however, the “dip” phenomenon was not observed in any velocity profiles, owing to the two-dimensional flows with large aspect ratio (Figure 11).

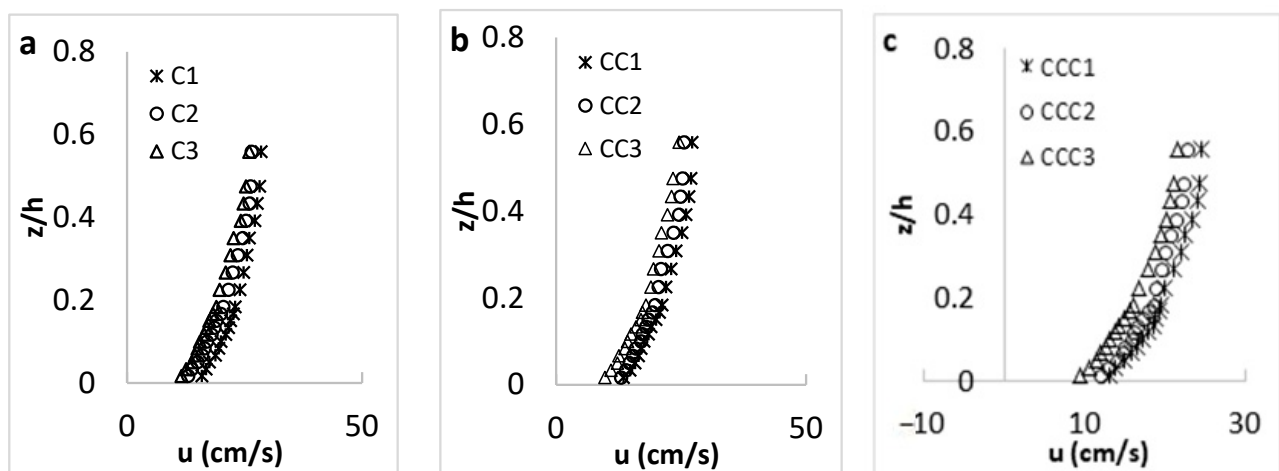


Figure 11. (a–c) Streamwise velocity distributions (experimental setup: $S = 0.015$, $d_{50} = 1.08$ mm).

3.2.2. Turbulence Intensity Distribution

The distributions of turbulence intensity of flow in the sloped channel with vegetated sidewalls for both sands of different particle sizes were similar to those of the experiments in the flat channel ($S = 0$), in which the maximum value of the turbulence intensity occurred at a distance close to the channel bed. The turbulence intensities increased by moving towards the flume sidewalls due to the generation of higher turbulence by the vegetated sidewalls (Figures 12 and 13).

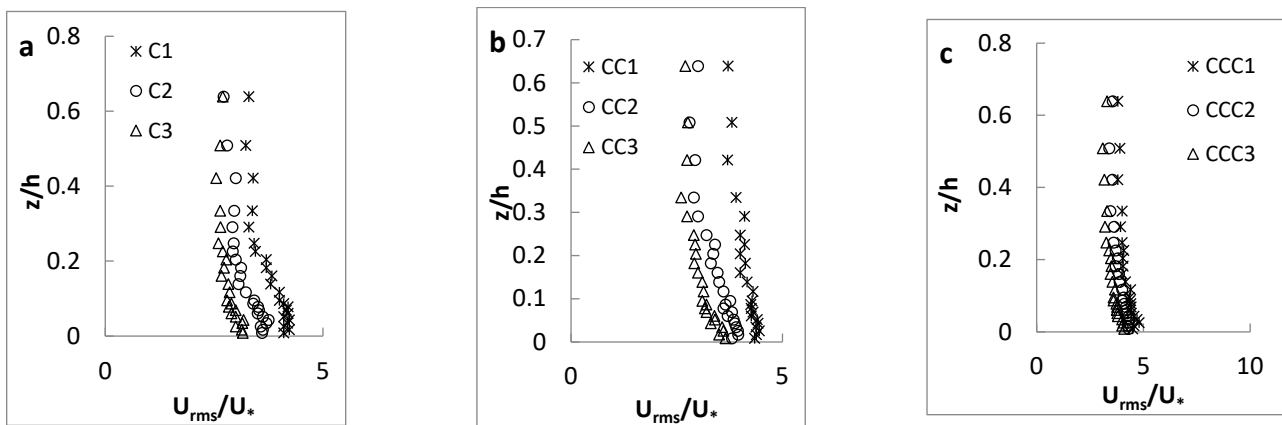


Figure 12. (a–c) Turbulence intensity distributions, (experimental setup: $S = 0.015$, $d_{50} = 0.56$ mm).

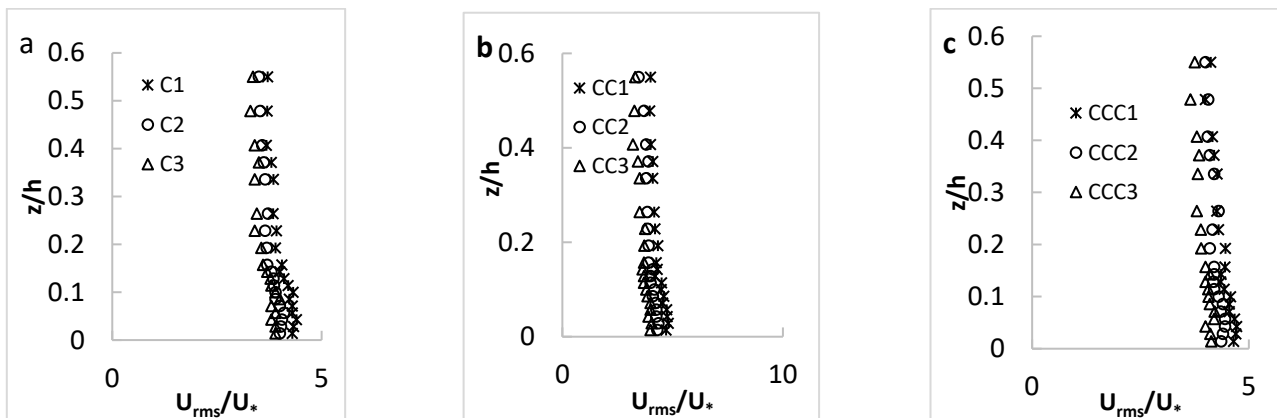


Figure 13. (a–c) Turbulence intensity distributions (experimental setup: $S = 0.015$, $d_{50} = 1.08$ mm).

3.2.3. Reynolds Shear Stress

The Reynolds shear stress distributions for flow in the channel with both the finest and coarsest sands as the bed material are shown in Figures 14 and 15, respectively. As observed from Figures 14 and 15, the distribution of Reynolds shear stress also had a Z-shape pattern, and the maximum value occurred at a larger distance from the channel bed by moving towards the channel walls. The Reynolds stresses in the spanwise direction can be observed by a variation of the maximum Reynolds stress location in each profile. Near the vegetation wall, the maximum Reynolds stress occurs near the bed; however, by moving toward the central axis of the flume, the effect of vegetation wall decreases leading to the occurrence of maximum Reynolds stress far from the channel bed. This variation is affected by both bed slopes and sediment sizes. The maximum Reynolds stress values had a descending trend from CS-1 to CS-3, due to the increase in the channel width and the presence of a positive slope (Note: the slope is in the flow direction). Results showed that the shear stress values in a channel with a steep bed slope were less than those in the flat channel (without bed slope) because less energy is required for initiating the movement of particles by increasing the bed slope.

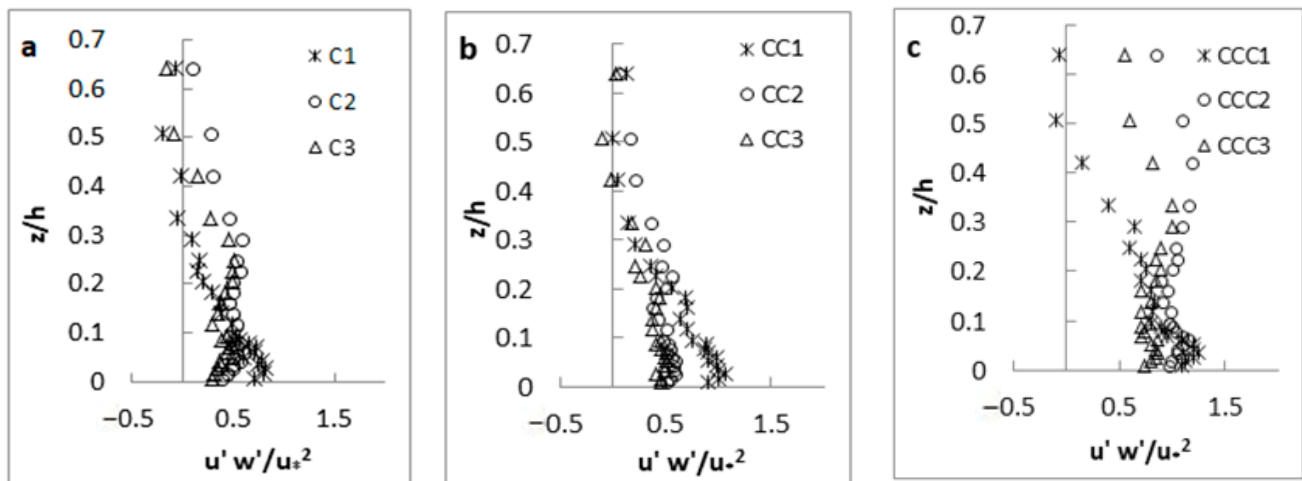


Figure 14. (a–c) Reynolds shear stress distributions (experimental setup: $S = 0.015$, $d_{50} = 0.56$ mm).

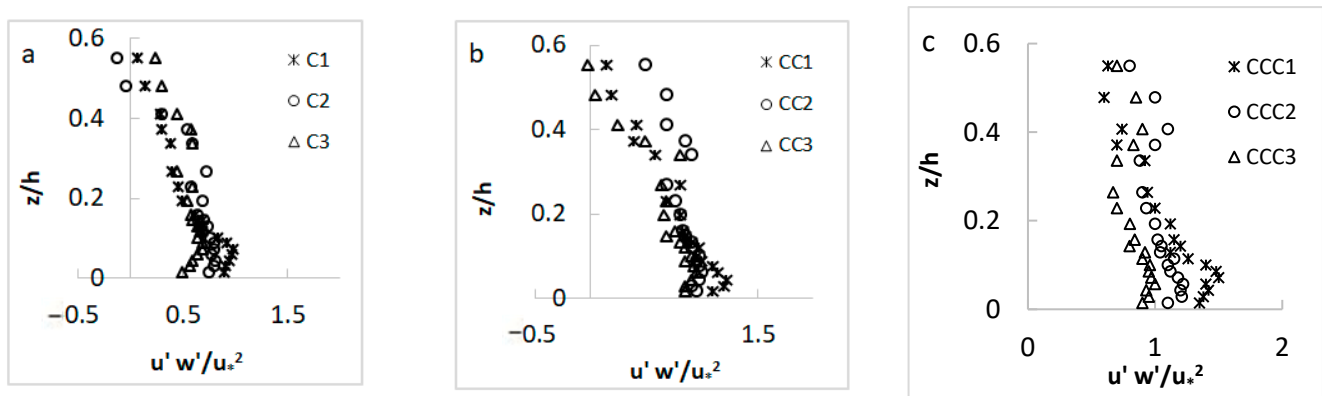


Figure 15. (a–c) Reynolds shear stress distributions (experimental setup: $S = 0.015$, $d_{50} = 1.08$ mm).

3.3. Determination of Incipient Near-Bed Velocity and Shear Stress

–0.5 It has been proven by several studies that the logarithmic law is valid for the velocity data in the inner layer near the bed ($z/h \leq 0.2$) in the presence of both submerged and emergent vegetation [9,21,36]. By fitting the logarithmic regression on the velocity data acquired in the inner layer of flows for all experimental runs for this research, it was observed that the coefficient of determination (R^2) was more than 93% for all velocity profiles (Table 2), confirming the validity of the logarithmic law.

Table 2. The logarithmic fitting equations for velocity profiles in the inner layer ($S = 0$).

Sand Types	Locations	Equations	R^2
I	C1	$u = 2.9882\ln\left(\frac{z}{h}\right) + 25.224$	0.9733
	C2	$u = 2.3769\ln\left(\frac{z}{h}\right) + 21.181$	0.9354
	C3	$u = 2.7077\ln\left(\frac{z}{h}\right) + 21.407$	0.9306
	CC1	$u = 1.1997\ln\left(\frac{z}{h}\right) + 16.096$	0.9432
	CC2	$u = 1.7241\ln\left(\frac{z}{h}\right) + 17.814$	0.9404
	CC3	$u = 1.0143\ln\left(\frac{z}{h}\right) + 15.175$	0.9305
	CCC1	$u = 1.3003\ln\left(\frac{z}{h}\right) + 17.146$	0.9391
	CCC2	$u = 1.0885\ln\left(\frac{z}{h}\right) + 16.235$	0.9304
	CCC3	$u = 1.6302\ln\left(\frac{z}{h}\right) + 17.542$	0.9221

Table 2. *Cont.*

Sand Types	Locations	Equations	R ²
II	C1	$u = 2.6512\ln\left(\frac{z}{h}\right) + 26.311$	0.9542
	C2	$u = 2.3201\ln\left(\frac{z}{h}\right) + 22.420$	0.9606
	C3	$u = 2.5632\ln\left(\frac{z}{h}\right) + 24.314$	0.9471
	CC1	$u = 2.0369\ln\left(\frac{z}{h}\right) + 23.204$	0.9325
	CC2	$u = 1.9264\ln\left(\frac{z}{h}\right) + 21.553$	0.94103
	CC3	$u = 1.2107\ln\left(\frac{z}{h}\right) + 18.087$	0.9564
	CCC1	$u = 1.7844\ln\left(\frac{z}{h}\right) + 22.566$	0.9567
	CCC2	$u = 2.2371\ln\left(\frac{z}{h}\right) + 26.952$	0.9378
	CCC3	$u = 2.0177\ln\left(\frac{z}{h}\right) + 25.912$	0.9422
III	C1	$u = 2.4561\ln\left(\frac{z}{h}\right) + 28.398$	0.963
	C2	$u = 2.3496\ln\left(\frac{z}{h}\right) + 26.942$	0.9343
	C3	$u = 2.2791\ln\left(\frac{z}{h}\right) + 22.312$	0.9321
	CC1	$u = 3.167\ln\left(\frac{z}{h}\right) + 27.64$	0.9507
	CC2	$u = 2.1834\ln\left(\frac{z}{h}\right) + 25.081$	0.9434
	CC3	$u = 1.895\ln\left(\frac{z}{h}\right) + 27.842$	0.9352
	CCC1	$u = 2.1113\ln\left(\frac{z}{h}\right) + 25.264$	0.9391
	CCC2	$u = 1.8907\ln\left(\frac{z}{h}\right) + 26.79$	0.9737
	CCC3	$u = 1.5701\ln\left(\frac{z}{h}\right) + 25.74$	0.934

By extrapolating the velocity profiles to the surface of the channel bed, the near-bed velocities for the incipient motion of different bed material have been determined. Several researchers proposed a formula for estimating the near-bed threshold velocity and shear stress. For instance, Garde [10] and Mavis & Laushey [11] proposed Equations (1) and (2), respectively:

$$u_{cr} = 1.51(\Delta g d)^{0.5} \tag{1}$$

$$u_{cr} = 3.3\Delta^{0.5} d^{4/9} \tag{2}$$

where u_{cr} is the near bed threshold velocity, $\Delta = s - 1$, ($s = \rho_s/\rho$), g is the gravity force, and d is the median diameter of particle.

As summarized in Table 3, the estimated near-bed velocities of the present study are compared to those calculated using the two equations above. As shown in Table 3 for both channel bed slopes, the estimated near-bed velocity values in the current study were closer to the results calculated by using the equation proposed by Mavis and Laushey [11]. Furthermore, the difference between the estimated results of this study and calculated values using the above equations reduced as the particle size of bed material increased, which can be attributed to the range of bed particles used for developing those equations. It can be seen that the errors using those two equations (compared to the estimated values from the current experiments) for the channel with the slope of $S = 0.015$ are more than those in the channel with a flatbed ($S = 0$).

Table 3. The estimation of the near-bed velocity based on laboratory experiments.

Methods	Bed Slope: $S = 0$			Bed Slope: $S = 0.015$		
	Particles					
	I	II	III	I	II	III
Experimental results	9.14	12.43	15.54	6.56	9.19	12.06
Garde (1970)	14.4	16.7	20	14.4	16.7	20
Error	36%	25%	22%	54%	44%	39%
Mavis & Laushey (1966)	11.8	13.3	15.8	11.8	13.3	15.8
Error	22%	6%	1.6%	36%	30%	23%

On the other hand, the incipient near-bed shear stress values were determined by extrapolating the Reynolds shear stress profiles towards the bed surface. The results of shear stress values are presented in Table 4.

Table 4. The summary of incipient velocity (u_{oc}) and shear stress (τ_{oc}) for different cases.

Bed Slope	Particle I: $d_{50} = 0.56$ mm		Particle II: $d_{50} = 0.74$ mm		Particle III: $d_{50} = 1.08$ mm	
	u_{oc} (cm/s)	τ_{oc} (N/m ²)	u_{oc} (cm/s)	τ_{oc} (N/m ²)	u_{oc} (cm/s)	τ_{oc} (N/m ²)
$S = 0$	9.14	0.071	12.43	0.099	15.54	0.195
$S = 0.0075$	7.54	0.067	10.21	0.092	13.28	0.172
$S = 0.015$	6.56	0.061	9.19	0.085	12.06	0.166

From the results of experiments conducted in the channel with different bed slopes, it can be observed that the initiation of particles on the channel bed becomes more difficult as the particle size increases. An increase in the size of a particle and the rise of its submerged weight required a larger hydrodynamic force to move the coarse particles. As a result, the incipient near-bed velocity and shear stress rose as the particle size increased, regardless of the bed slope. This finding agrees with the results of other studies [9,15,16].

For investigating the effects of the bed slope on the near-bed parameters for the incipient motion of bed material, it is found that the bed slope has an impact on the incipient movement of particles in two opposing ways, which is classified as the “pressure gradient” and “gravity” impacts. With a positive bed slope (decelerating flow), a negative velocity gradient or positive pressure gradient exists. Resultantly, it becomes more difficult for bed particles to be initiated to move (pressure gradient effect). However, the steeper positive bed slope renders particle motion easier since the particles move downward, directed by gravity (gravity effect). In several previous studies in which the impact of the slope of a channel bed on the initiation of bed particles was investigated, it was revealed that the pressure gradient effect was more dominant than the gravity effect. In other words, as the adverse (negative) slope steepens, the critical Shields parameter decreases, and, subsequently, the particle movements become easier, and vice versa [15,16,36]. In this study, however, the opposite behavior was observed, since the incipient near-bed velocity and shear stress increased by steepening the positive bed slope. It may be the influence of the simultaneous presence of the varying channel width and vegetation on the channel sidewalls. In other words, the non-uniform flow along the channel caused the dominance of gravity effects in the current research.

3.4. Estimation of Shields Parameter

As mentioned in the introduction section, the Shields method relies on computing the critical shear Reynolds number (R_{*c}) and Shields dimensionless parameter (θ_c), which can be calculated as follows [14]:

$$R_{*c} = \frac{u_* d}{\nu} \tag{3}$$

$$\theta_c = \frac{\tau_{0c}}{(\rho_s - \rho)gd} \tag{4}$$

where $u_* = \sqrt{\tau_{0c}/\rho}$ is the shear velocity, and τ_{0c} is the critical bed shear stress.

Table 5 summarizes the values of critical shear Reynolds number and Shields dimensionless parameter calculated using Equations (3) and (4). The trend of the Shields parameter values is in accordance with that of the near-bed velocity and shear stress for the incipient motion of bed material, namely the Shields parameter values increase by increasing the particle size and by decreasing the bed slope, indicating more difficulties to initiate the movement of the bed particles.

Table 5. The critical shear Reynolds number and shields dimensionless parameter values.

Bed Slope	Particle I: $d_{50} = 0.56 \text{ mm}$		Particle II: $d_{50} = 0.74 \text{ mm}$		Particle III: $d_{50} = 1.08 \text{ mm}$	
	θ_c	R_{*c}	θ_c	R_{*c}	θ_c	R_{*c}
$S = 0$	0.007	4.70	0.008	7.33	0.011	15.01
$S = 0.0075$	0.007	4.58	0.008	7.09	0.010	14.15
$S = 0.015$	0.0067	4.37	0.007	6.82	0.009	13.91

By locating the critical shear Reynolds number and Shields parameter values on the Shields diagram, it was expected that the data points should lie on the Shields curve, indicating the threshold condition. However, as shown in Figure 16, it is observed that all estimated data points were placed below the Shields curve in the range for “no sediment motion”, indicating the invalidity of the Shields approach for assessing the incipient motion in this research, due to the following reasons:

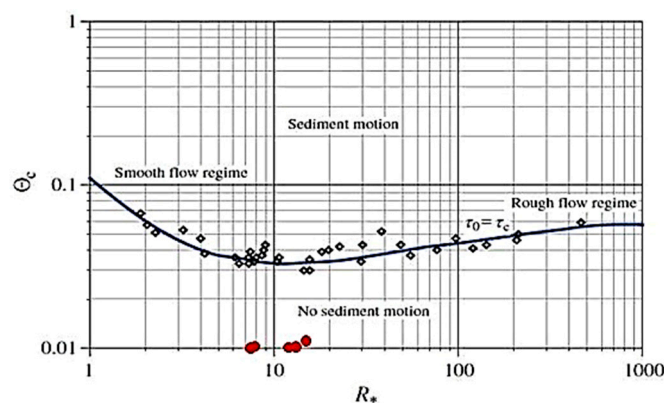


Figure 16. The measured data of this study on the Shields diagram (circle dot symbol).

- (1) The difference between the definitions of the threshold condition: Shields employed the general motion criteria of the Kramer method in his research [41]. In the present work, however, the medium transport criterion of the Kramer approach was applied, without formation of any bedforms. Different approaches for assessing the incipient motion of bed material may lead to various critical shear stress values. Generally, the presence of bedforms affects the bed near-bed shear stress and sediment transport by exerting more turbulence and drag force [42]. In previous studies, it was proved

that the negligible differences in water level over the bedforms may cause some overestimation of shear stress [42–44]. Furthermore, the dissipation of bed shear stress due to presence of bedforms leads to a remarkable overestimation in determining bed shear stress.

- (2) Different experimental setups: experiments in Shields' study were carried out in a prism channel without any changes in the channel width and without presence of vegetation. These changes in the present work led to an increase in turbulence intensities, which play a key role in lifting particles from the channel bed. Hence, the bed shear stress needed to render the bed particles' motion decreases significantly.
- (3) Characteristics of bed particle: Shields used four types of sub-angular to very angular particles in his experiments. On the other hand, naturally rounded quartz particles were applied in the current research. Angular particles used in the Shields' study led to more resistance to incipient movements, owing to producing more friction [15], and thus a significant increase in the critical shear stress.
- (4) Accuracy of measurement: The measuring tools for experiments in this study are more advanced and accurate, compared to those employed by Shields a long time ago. Resultantly, it is expected to estimate the critical shear stress more precisely comparing to that reported by Shields [14].

Despite extensive applications of the Shields diagram, several researchers had also challenged its validity in various experimental setups [9,16,45–47]. In some previous experimental studies about the incipient motions of particles, it was reported that the Shields diagram was not valid in different cases, including the presence of both decelerating and accelerating flows [15,16], and the presence of vegetation patches over the bed [9]. It should be noted that some results of the present study agree with other studies. For instance, the results of the current study show that the Shields diagram is not a suitable choice to predict the incipient motion, due to the statements made by other researchers for different experimental conditions, including the non-uniform flow in non-vegetated channels [15,16]. However, the presence of wall vegetation leads to different Reynolds stress distribution. The results of this study show that any estimation of critical movement of bed material, drag or Manning coefficients may not be valid by using the traditional methods for determining the shear stress. For example, for streams without the presence of vegetation, the present knowledge suggests that the shear stress has a linear or convex distribution near the channel bed over sand and gravel bed streams. However, in this study, a Z-shaped shear stress distribution is observed in the presence of wall vegetation. Results showed that there exists an increasing trend in Reynolds stress toward the water surface in some figures or different patterns in the inner (near the bed) and outer layers (near the water surface) of the boundary layer in each Reynolds stress distribution. Thus, the interaction of channel width variation with wall vegetation is a complex issue and cannot be explained by simplification of the Reynolds momentum equation. The results show that the wall vegetation plays a significant role on the incipient motion of bed material via the shear stress estimation. In fact, the application of the Reynolds shear stress in the nominator of a Shields parameter may not correctly show the effect of the important factors influencing the threshold condition. Moreover, the comparison of the Shields diagram is improved in the revised manuscript.

4. Conclusions

The present study aims to investigate the impacts of the varying width and vegetated sidewalls of the channel on flow structures under the condition of the incipient motion of particles in the channel bed. The total of 9 experiments with different setups has been carried out by changing the channel width, particle size of bed material and bed slope. The following results have been drawn from this study:

- (1) As expected, the streamwise velocity had its maximum and minimum values at the narrowest CS (CS-1) and widest CS (CS-3), respectively, along all axes (C-axis, CC-axis and CCC-axis). Additionally, in cases with an aspect ratio of $w/h < 5$, the maximum

velocity occurred below the water surface (“dip” phenomenon), owing to the presence of secondary currents.

- (2) The turbulence intensity started from a non-zero value, increased until reached its maximum value at a distance near the bed, and then had a descending trend towards the water surface. The presence of vegetation on the channel sidewalls resulted in an increasing trend of the turbulence intensity while moving from the central C-axis to the channel sidewalls.
- (3) The distribution of Reynolds shear stress had a Z-shape profile at all measurement points, due to presence of vegetation on the channel sidewalls. The maximum values of the Reynolds shear stress at CS-2 and CS-3 occurred at the flow depth of $0.3 < z/h < 0.4$ from the channel bed, where the flow decelerated along this channel section from CS-2 to CS-3.
- (4) The incipient near-bed velocity and shear stress increased by increasing the particle size. On the other hand, the estimated near-bed velocity and shear stress decreased with the increase in the bed slope, which represents the dominance of the gravity effect over the pressure gradient effect. It can be inferred that the variation of the channel width and the presence of vegetation on the channel sidewalls remarkably influences the turbulence intensity and Reynolds shear stress distributions.
- (5) By locating the critical shear Reynolds number and Shields parameter values on the Shields diagram, it was observed that all estimated data points were placed below the Shields curve in the range for “no sediment motion”, indicating the invalidity of the Shields approach for assessing the incipient motion in this research with the presence of varying channel width and vegetated channel sidewalls.

Estimations of the important parameters of fluvial hydraulics, such as flow resistance and sedimentation rate, are based on measured data under complicated conditions of a natural river, including variations of channel width and the presence of vegetation patches in a channel. This research is in initial step of the fluvial hydraulics in channels with varying width in the presence of emergent vegetation on the channel sidewalls. To the authors’ knowledge, no research works in literature have been conducted to study the characteristics of turbulent flow under the condition of the incipient motion of bed material in a channel with varying width and vegetated channel walls. That is the reason for a simple experimental setup in order to investigate whether the wall vegetation affects the shear stress and, consequently, the incipient motion of bed material. This simplification includes the use a symmetric width variation along the flume with uniform emergent wall vegetation cover. Since the selection of the Reynolds stress distribution (Z-shaped, or complex convex shaped distributions) significantly influences the estimation of the critical condition of sediment movement, any over- or under-estimation of Reynolds stress misleads engineers in river engineering projects, including the unreasonable cost and feasibility of any restoration projects. The results of this study can be used as the reference for estimating the drag coefficient in rivers with varying channel width and emergent vegetation on channel banks and floodplains.

Author Contributions: Conceptualization, S.H. and H.A.; methodology, S.H. and H.A.; validation, S.H.; investigation, S.H., H.A. and J.S.; data curation, H.A. and J.S.; writing—original draft preparation, S.H.; writing—review and editing, H.A. and J.S. All authors have read and agreed to the published version of the manuscript.

Funding: This research received no external funding.

Institutional Review Board Statement: Not applicable.

Informed Consent Statement: Not applicable.

Data Availability Statement: The data that support the findings of this study are available upon reasonable request.

Conflicts of Interest: The authors declare no conflict of interest.

References

1. Wang, J.; Sui, J.; Karney, B.W. Incipient motion of non-cohesive sediment under ice cover—an experimental study. *J. Hydrodyn.* **2008**, *20*, 117–124. [[CrossRef](#)]
2. Church, M.; Hassan, M. Upland gravel-bed rivers with low sediment transport. In *643 Catchment Dynamics and River Processes, Mediterranean and other Climate Regions 644, Developments in Earth Surface Processes*; Elsevier: Amsterdam, The Netherlands, 2005; Volume 7, pp. 141–168.
3. Garcia, C.; Laronne, J.B.; Sala, M. Variable source areas of bedload in a gravel bed stream. *J. Sediment. Res.* **1999**, *69*, 2–31. [[CrossRef](#)]
4. Dey, S. *Fluvial Hydrodynamics: Hydrodynamic and Sediment Transport Phenomena*; Springer: Berlin/Heidelberg, Germany, 2014; pp. 158–162.
5. Buffington, J.M.; Montgomery, D.R. A systematic analysis of eight decades of incipient motion studies, with special reference to gravel-bedded rivers. *Water Resour. Res.* **1997**, *33*, 1993–2029. [[CrossRef](#)]
6. Wilcock, P.R. Methods for estimating the critical shear stress of individual fractions in mixed-size sediment. *Water Resour. Res.* **1988**, *24*, 1127–1135. [[CrossRef](#)]
7. Kramer, H. Sand mixtures and sand movement in fluvial model. *Trans. Am. Soc. Civ. Eng.* **1935**, *100*, 798–838. [[CrossRef](#)]
8. Dey, S.; Sarkar, S.; Solari, L. Near-bed turbulence characteristics at the entrainment threshold of sediment beds. *J. Hydraul. Eng.* **2011**, *137*, 945–958. [[CrossRef](#)]
9. Shahmohammadi, R.; Afzalimehr, H.; Sui, J. Impacts of turbulent flow over a channel bed with a vegetation patch on the incipient motion of sediment. *Can. J. Civ. Eng.* **2018**, *9*, 803–816. [[CrossRef](#)]
10. Garde, R.J. Initiation of motion on a hydrodynamically rough surface—Critical velocity approach. *J. Irrig. Power* **1970**, *27*, 271–282.
11. Mavis, F.T.; Laushey, L.M. Discussion of “Sediment transportation mechanics: 662 Initiation of motion”. *ASCE J. Hydraul. Div.* **1966**, *92*, 288–291.
12. Wang, H.; Tang, H.W.; Zhao, H.Q.; Zhao, X.Y.; Lu, S.Q. Incipient motion of 675 sediment in presence of submerged flexible vegetation. *Water Sci. Eng.* **2015**, *676*, 63–67. [[CrossRef](#)]
13. Zanke, U.C.E. Neuer ansatz zur berechnung des transportbeginns von sedimenten unter stromungseinfluss. *Mitteilungen Des Franzius-Inst. Tech. Univ. Hann.* **1977**, *46*, 156–178.
14. Shields, A.F. *Application of Similarity Principles and Turbulence Research to Bed-Load Movement*; Mitteilungen der Preussischen Versuchsanstalt für Wasserbau und Schiffbau: Berlin, Germany, 1936; Volume 26, pp. 5–24.
15. Bolhassani, R.; Afzalimehr, H.; Dey, S. Effects of relative submergence and bed slope on sediment incipient motion under decelerating flows. *J. Hydrol. Hydromech.* **2015**, *63*, 295–302. [[CrossRef](#)]
16. Emadzadeh, A.; Meng Chiew, Y.; Afzalimehr, H. Effect of accelerating and decelerating flows on incipient motion in sand bed streams. *Adv. Water Resour.* **2010**, *33*, 1094–1104. [[CrossRef](#)]
17. King, A.T.; Tinoco, R.O.; Cowen, E.A. A $k-\epsilon$ turbulence model based on the scales of vertical shear and stem wakes valid for emergent and submerged vegetated flows. *J. Fluid Mech.* **2012**, *701*, 1–39. [[CrossRef](#)]
18. Mofrad, M.R.; Afzalimehr, H.; Parvizi, P.; Ahmad, S. Comparison of Velocity and Reynolds Stress Distributions in a Straight Rectangular Channel with Submerged and Emergent Vegetation. *Water* **2023**, *15*, 24–35. [[CrossRef](#)]
19. Tang, H.W.; Wang, H.; Liang, D.F.; Lv, S.Q.; Yan, L. Incipient motion of sediment in the presence of emergent rigid vegetation. *J. Hydro-Environ. Res.* **2012**, *7*, 1–7.
20. Yang, J.; Chung, H.; Nepf, H. The onset of sediment transport in vegetated channels predicted by turbulent kinetic energy. *Geophys. Res. Lett.* **2016**, *43*, 11, 261–268. [[CrossRef](#)]
21. Soltani, N.; Afzalimehr, H.; Tabarestani, E.S.; Eftekhari, A.; Khabari, M.; Nazari-Sharabian, M.; Karakouzian, M. Turbulence Characteristics in Mild and Steep Entrance Slopes of Pool-Riffle Sequences. *Water* **2023**, *15*, 720. [[CrossRef](#)]
22. Xiao, B.; Wang, W.; Zhang, X.; Long, G.; Fan, J.; Chen, H.; Deng, L. A novel fractal solution for permeability and Kozeny-Carman constant of fibrous porous media made up of solid particles and porous fibers. *Powder Technol.* **2019**, *1*, 92–98. [[CrossRef](#)]
23. Xiao, B.; Zhu, H.; Chen, F.; Long, G.; Li, Y. A fractal analytical model for Kozeny-Carman constant and permeability of roughened porous media composed of particles and converging-diverging capillaries. *Powder Technol.* **2023**, *15*, 118256. [[CrossRef](#)]
24. Nelson, P.A.; Brew, A.K.; Morgan, J.A. Morphodynamic response of a variable-width channel to changes in sediment supply. *Water Resour. Res.* **2015**, *51*, 5717–5734. [[CrossRef](#)]
25. Morgan, J.A. The Effects of Sediment Supply, Width Variations, and Unsteady Flow on Riffle-Pool Dynamics. Ph.D. Thesis, Department of Civil and Environmental Engineering, Colorado State University, Fort Collins, CO, USA, 2018.
26. Shahiri Tabarestani, E.; Afzalimehr, H.; Sui, J. Assessment of Annual Erosion and Sediment Yield Using Empirical Methods and Validating with Field Measurements—A Case Study. *Water* **2022**, *14*, 1602. [[CrossRef](#)]
27. Repetto, R.; Tubino, M.; Paola, C. Planimetric instability of channels with variable width. *J. Fluid Mech.* **2002**, *457*, 79–109. [[CrossRef](#)]
28. Chartrand, S.M.; Jellinek, A.M.; Hassan, M.A.; Ferrer-Boix, C. Morphodynamics of a width-variable gravel bed stream: New insights on pool-riffle formation from physical experiments. *J. Geophys. Res. Earth Surf.* **2018**, *123*, 2735–2766. [[CrossRef](#)]
29. Shahiri Tabarestani, E.; Afzalimehr, H.; Pham, Q.B. Flow structure investigation over a pool-riffle sequence in a variable width river. *Acta Geophys.* **2022**, *70*, 713–727. [[CrossRef](#)]

30. Viparelli, E.; Gaeuman, D.; Wilcock, P.; Parker, G. A model to predict the evolution of a gravel bed river under an imposed cyclic hydrograph and its application to the Trinity River. *Water Resour. Res.* **2011**, *47*, 1–22. [[CrossRef](#)]
31. PPace, K.M.; Tullos, D.; Walter, C.; Lancaster, S.; Segura, C. Sediment Pulse Behaviour Following Dam Removal in Gravel-Bed Rivers. *River Res. Appl.* **2017**, *33*, 102–112. [[CrossRef](#)]
32. Nelson, P.A.; Venditti, J.G.; Dietrich, W.E.; Kirchner, J.W.; Ikeda, H.; Iseya, F.; Sklar, L.S. Response of bed surface patchiness to reductions in sediment supply. *J. Geophys. Res. Earth Surf.* **2009**, *114*, 1–18. [[CrossRef](#)]
33. Maturana, O.; Tonina, D.; McKean, J.A.; Buffington, J.M.; Luce, C.H.; Caamaño, D. Modeling the effects of pulsed versus chronic sand inputs on salmonid spawning habitat in a low-gradient gravel-bed river. *Earth Surf. Process. Landf.* **2014**, *39*, 877–889. [[CrossRef](#)]
34. Parker, G. 1D Sediment Transport Morphodynamics with Applications to Rivers and Turbidity Currents. 2006. Available online: https://csdms.colorado.edu/wiki/1D_Sediment_Transport_Morphodynamics_with_applications_to_Rivers_and_Turbidity_Currents (accessed on 13 April 2006).
35. Absi, R. An ordinary differential equation for velocity distribution and dip-phenomenon in open channel flows. *J. Hydraul. Res.* **2011**, *49*, 82–89. [[CrossRef](#)]
36. Afzalimehr, H.; Dey, S. Influence of bank vegetation and gravel bed on velocity and Reynolds stress distributions. *Int. J. Sediment Res.* **2009**, *24*, 236–246. [[CrossRef](#)]
37. Grass, A.J. Structural features of turbulent flow over smooth and rough boundaries. *J. Fluid Mech.* **1971**, *50*, 233–255. [[CrossRef](#)]
38. Hadian, S.; Afzalimehr, H.; Ahmad, S. Effects of Channel Width Variations on Turbulent Flow Structures in the Presence of Three-Dimensional Pool-Riffle. *Sustainability* **2023**, *15*, 7829. [[CrossRef](#)]
39. Nepf, H.M.; Vivoni, E.R. Turbulence structure in depth-limited vegetated flow: Transition between emergent and submerged regimes. In Proceedings of the 28th IAHR Congress, Graz, Austria, August 1999; pp. 1–8.
40. Nikora, V.I.; Goring, D.G. ADV measurements of turbulence: Can we improve their interpretation? *J. Hydraul. Eng.* **1998**, *124*, 630–634. [[CrossRef](#)]
41. Kennedy, J.F. The Albert Shields story. *J. Hydraul. Eng.* **1995**, *121*, 766–772. [[CrossRef](#)]
42. Buffington, J.M. The legend of AF Shields. *J. Hydraul. Eng.* **1999**, *125*, 376–387. [[CrossRef](#)]
43. Parker, G.; Peterson, A.W. Bar resistance of gravel-bed streams. *J. Hydraul. Div.* **1980**, *106*, 1559–1575. [[CrossRef](#)]
44. Hey, R.D. Bar form resistance in gravel-bed rivers. *J. Hydraul. Eng.* **1988**, *114*, 1498–1508. [[CrossRef](#)]
45. Dey, S.; Papanicolaou, A. Sediment threshold under stream flow: A state-of-the-art review. *KSCE J. Civ. Eng.* **2008**, *12*, 45–60. [[CrossRef](#)]
46. Paphitis, D. Sediment movement under unidirectional flows: An assessment of empirical threshold curves. *Coast Eng.* **2001**, *43*, 227–245. [[CrossRef](#)]
47. Diplas, P. Bed load transport in gravel-bed streams. *J. Hydraul. Eng.* **1987**, *113*, 277–292. [[CrossRef](#)]

Disclaimer/Publisher’s Note: The statements, opinions and data contained in all publications are solely those of the individual author(s) and contributor(s) and not of MDPI and/or the editor(s). MDPI and/or the editor(s) disclaim responsibility for any injury to people or property resulting from any ideas, methods, instructions or products referred to in the content.